

Spectroscopy of silica layers containing Si nanocrystals: Experimental evidence of optical birefringence

Leonid Khriachtchev^{a)}*Laboratory of Physical Chemistry, University of Helsinki, P.O. Box 55, Helsinki FIN-00014, Finland*

Daniel Navarro-Urrios and Lorenzo Pavesi

Dipartimento di Fisica, Università di Trento, Via Sommarive 14, 38050 Povo, Italy

Claudio J. Oton and Nestor E. Capuj

Departamento de Fisica Basica, University of La Laguna, Tenerife, 38204 La Laguna, Spain

Sergei Novikov

*Electron Physics Laboratory, Helsinki University of Technology, P.O. Box 3000,**Helsinki FIN-02015 HUT, Finland*

(Received 19 June 2006; accepted 28 November 2006; published online 27 February 2007)

We report an unusual case of spectral filtering by a silica waveguide containing Si nanocrystals (Si-nc's) deposited on a silica plate. For a number of Si-rich silica (SiO_x) slab waveguides annealed at 1100 °C, the TE and TM waveguide mode cutoff positions are found in the inversed order with respect to the classical waveguide theory for an isotropic material. Using the cutoff and m -line spectra, this unusual behavior was explained assuming an optical birefringence of the material. For the highest Si content ($x \sim 1.5$), we estimated a maximal positive birefringence of $\sim 8\%$. The cutoff spectrum simulated with the optical parameters extracted from the m -line measurements corresponds well to the cutoff spectrum directly obtained by measuring waveguided luminescence. This agreement shows that the spectral filtering effect of silica layers containing Si-nc can be described within the quantitative model of delocalized waveguide modes. The possible origin for the observed birefringence is discussed. © 2007 American Institute of Physics.

[DOI: [10.1063/1.2433136](https://doi.org/10.1063/1.2433136)]

I. INTRODUCTION

Optical and electronic properties of silicon strongly depend on its structure on the nanometer scale.^{1,2} In fact, strong room temperature visible light emission from silica layers containing Si nanocrystals (Si-nc's) is possible, which motivates a large interest in these systems for nanophotonics. The interest is also motivated by recent reports on optical gain in related materials.³⁻⁵ A suggested model for the broad photoluminescence (PL) around 1.6 eV (~ 800 nm) as well as for the optical gain in the same spectral region is based on localized-state recombination involving Si=O covalent bonds.² The PL spectrum of Si-nc embedded in SiO_2 was found to be quite independent of the Si-nc diameter, which supported the "surface-state model" for the light emission.⁶ In analogy with oxidized porous Si,⁷ the oxygen-related light-emitting centers would be at the interface area between Si-nc and the host oxide. This image finds support in the synchronous crystallization of Si and enhancement of the 1.6 eV PL upon thermal annealing above 1000 °C, which is often observed experimentally for various Si/ SiO_2 materials. However, some experiments have shown that the 1.6 eV PL can be intense in annealed Si/ SiO_2 materials without obvious presence of Si-nc embedded in the oxide matrix.⁸⁻¹⁰ Thus, the light-emitting centers can be accommodated in a less ordered structure, which is invisible by Raman spectroscopy.¹¹⁻¹³ In addition to the emission properties,

Si-nc in silica can be used to increase the refractive index of the layer. Hence Si-nc in a silica layer on top of another silica layer can be used to form a planar waveguide when Si-nc rich silica layer forms the core waveguide layer.

It has been found that the guiding of Si-nc emitted luminescence by an annealed Si-rich silica (SiO_x) layer is wavelength selective.⁴ While the PL is broadband and mainly unpolarized, quite narrow and polarized spectral peaks are seen when guided light is detected, i. e., when the spectrum is measured from the waveguide edge. This effect, named also spectral filtering effect, has been observed for silica layers containing Si-nc, prepared with various methods (Si-rich silica, Si implantation, and Si/ SiO_2 superlattices).^{4,12,14-20} Two models have been suggested to interpret this effect: (i) the dependence of mode localization on the generalized frequency of the waveguide¹⁴⁻¹⁶ and (ii) the presence of quasiguided modes escaping the core layer.^{19,20} These two models are both based on the waveguide cutoff spectra and on the presence of a transparent cladding layer while the core layer is lossy. Experiments with free-standing films support these findings.¹²

In the present work, we report an unusual case of the spectral filtering effect by silica layers containing Si-nc, where the spectral positions of the TE and TM modes do not follow the classical waveguide theory for an isotropic slab waveguide. This behavior is explained by the optical birefringence of the core material.

^{a)}Electronic mail: leonid.khriachtchev@helsinki.fi

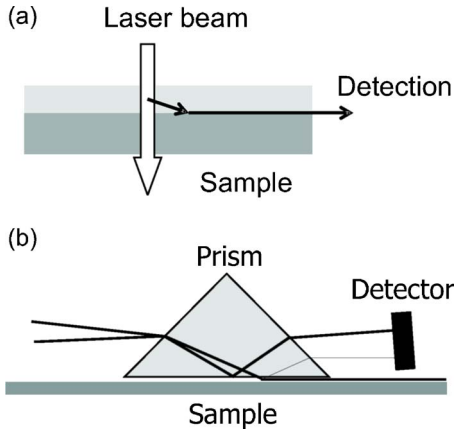


FIG. 1. (a) Detection of cutoff spectra. (b) Schematics of the m -line method.

II. EXPERIMENTAL DETAILS

This study is performed on various silicon rich silica (SiO_x) samples deposited by a reactive Si deposition method on 1-mm-thick silica plates.^{10,11,15} The most detailed measurements were done with a SiO_x optical wedge annealed at 1100 °C in nitrogen atmosphere for 1 h (sample 1). For this sample, the SiO_x layer has a gradient of the Si concentration along the sample surface, hence the name of optical wedge for this kind of samples is used. This gradient was achieved by using a nonperpendicular geometry between the Si beam axis and the substrate. In this situation, the distance from the Si source to the deposition area changes along the sample surface. The change of the x parameter due to this deposition asymmetry with respect to the central value was estimated to be $\pm 8\%$ and the central value of x was estimated to be 1.65. Some change in the layer thickness along the samples was also expected. These estimates were confirmed by optical and X-ray photoelectron spectroscopy measurements.^{11,15} Slices (~ 7 cm long) were cut along the Si concentration gradient through the sample center. By definition, we measure the displacement D along the cut from the sample side with the highest Si content. A number of other SiO_x samples were also used in the analysis, as specifically described below.

The PL measurements were performed using an Ar^+ laser (488 nm, Omnichrome 543-AP) and a He–Ne laser (633 nm, Uniphase 1145P) as excitation sources and a spectrometer (Acton SpectraPro 500I) equipped with a charge-coupled device camera (Andor InstaSpec IV). A particular geometry was used to detect the guided PL shown in Fig. 1(a).^{14–20} The excitation was done by using normal incidence (~ 0.5 mm in diameter), while the collection was done by using an objective from the sample edge with a collection spot of ~ 0.25 mm in diameter. The PL light exiting the waveguide sample in the direction nearly parallel to the sample surface was detected.¹⁵ The angular dependence of the filtering effect was studied by Valenta *et al.* elsewhere.^{18,19} According to Fermat's principle, the light propagating normal to the refractive index gradient tends to travel towards the higher refractive index; however, the difference of the trajectories for the TE and TM lights is negligible in the present case (less than 1 μm).

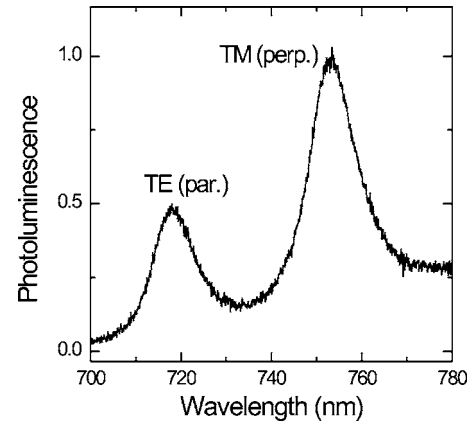


FIG. 2. Guided photoluminescence spectrum (sample 1) for displacement $D=2$ cm. TE and TM refer to the polarization of the luminescence.

In addition, we studied the samples with the m -line prism coupling technique shown in Fig. 1(b).²¹ With this method, an accurate characterization of waveguide optical modes can be performed and the refractive index of thin layers can be extracted. In our setup we used the 632.8 nm radiation of a He–Ne laser. The angular dependence of the reflectance of the beam is measured by a large area Si photodiode, and each guided mode is observed as a sharp dark peak in the reflectance spectra. The effective index of each guided mode is obtained from the incident angle and the refractive index of the prism from the following equation:

$$\beta(\theta_0) = n_p \sin \theta_0, \quad (1)$$

where β is the effective index of the mode, n_p is the refractive index of the prism, and θ_0 is the incidence angle.

III. EXPERIMENTAL RESULTS AND DISCUSSIONS

A. Cutoff spectra

Figure 2 shows the guided PL spectrum of sample 1 measured in a position $D=2$ cm. The two polarized peaks are a consequence of the spectral filtering of PL light since the emission is propagating in the waveguide. The model, which some of us proposed a few years ago, considers delocalization of guided modes near the mode cutoff.^{14–16} The mode localization is a function of the generalized frequency parameter which is written for an asymmetrical waveguide in the form

$$V = 2\pi(n_1^2 - n_2^2)^{1/2}d/\lambda, \quad (2)$$

where n_1 and n_2 are the refractive indices of the core layer and the cladding substrate, respectively, d is the core layer thickness, and λ is the wavelength.²² Optical confinement of the waveguide mode is minimum at the cutoff condition $V = (2m+1)\pi/2$. If the waveguide core layer has a large loss coefficient α_{core} and the substrate cladding layers has a small loss coefficient α_{sub} , then the modes near the cutoff suffer minimal losses. Equation (2) yields the cutoff wavelengths. For these wavelengths, intense PL is measured in the guided PL spectrum and the recorded light propagates mainly in the transparent substrate.

The central observation of the present work concerns the relative positions of the two polarized peaks measured in the guided PL spectrum. The theory for an isotropic asymmetrical waveguide predicts the TE modes (polarization parallel to the sample surface) to be at longer wavelengths (lower energies) than the TM modes (polarization perpendicular to the sample surface), while the spectral splitting between the modes depends on the difference of refractive indices of the core layer and substrate.²² In general, this is due to the different phase shifts for the TE and TM lights in Maxwell's equations for an isotropic asymmetrical waveguide. In the classical terminology of Kogelnik and Ramaswamy,²³ it is described as a difference of the asymmetry measure that is larger for the TM modes by a factor of $(n_1)^4$. The TE mode is better confined, except for very high filling factors, due to the strong asymmetry of the air-clad waveguide.²⁴ At odds with what we observed previously,^{14,16} the optical wedge exhibits a different ordering of the TE and TM peaks. In Fig. 2, the TE modes are at shorter wavelengths (higher energy) than the TM peaks. Figure 3(a) reports a summary of all the guided PL measurements: the polarized resolved emission peaks taken in various sample positions. The inverse ordering of TE and TM modes is obvious for great D , i.e., for the optically thinner part of the sample. A rather equidistant peak sequence is observed for small D , i.e., at the optically thicker part of the sample. To explain this ordering, we initially supposed that TE and TM modes of different orders could be mixed up due to the high refractive index of the core layer compared to the substrate. However, simple modeling shows that the peaks presented in Fig. 2 are of the same interference order.

To explain the observed cutoff spectra, we suggest the presence of optical birefringence of the core material. Within this model, the energy spacing between the cutoff positions for the two polarizations is different: it is larger for the TE than for the TM modes. In this situation, the TE peaks gradually appear at shorter wavelength (higher energy) than the TM peaks for waveguide mode order $m \gg 1$. It follows that the refractive index is smaller for the TE light (ordinary refractive index) than it is for the TM light (extraordinary refractive index), which means a positive birefringence.

This qualitative picture can be put onto a quantitative basis. The optical thickness of the layer can be measured from the interference pattern in the transmission spectra. The result of these measurements is shown in Fig. 3(b) as a function of the position on the optical wedge. The refractive index relevant to the transmission measurements is the TE refractive index. Thus, the TE refractive index can be extracted together with the layer thickness from the transmission spectra and the TE peaks, as described elsewhere.^{14–16} The obtained results are reported in Figs. 3(b) and 3(c). Next, we use the extracted layer thickness and the TM peak positions in order to obtain the refractive index for the TM light, and the result is shown in Fig. 3(c). It is found that the refractive index for the TM polarization is significantly larger than for the TE polarization. Figure 3(d) presents the relative difference of the two refractive indices (birefringence). The measured birefringence increases with the Si content, being $\sim 5\%$ at the sample edge with the highest Si concentration (

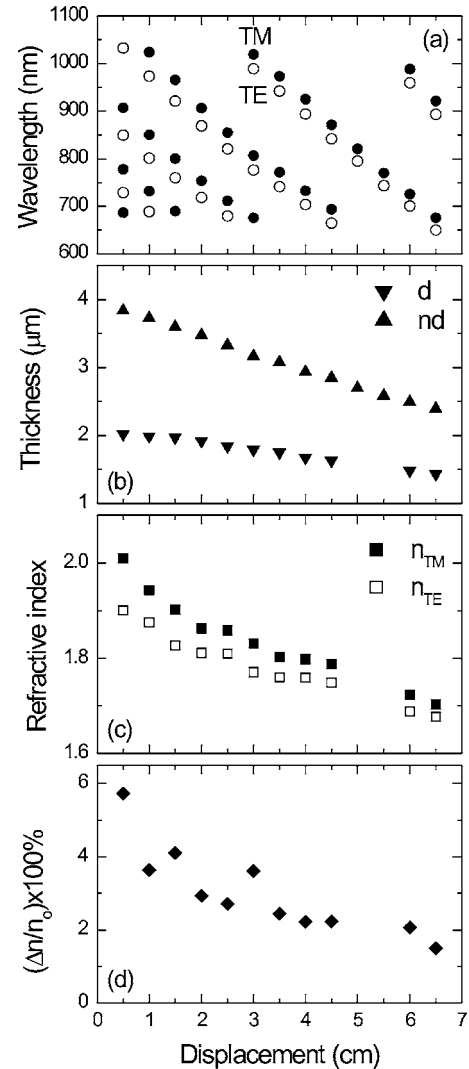


FIG. 3. (a) Positions of the TE (circles) and TM (disks) peaks as a function of displacement along the optical wedge surface (sample 1). (b) Optical thickness obtained from the transmission spectra and corresponding layer thickness. (c) Extracted n_{TE} and n_{TM} refractive indices at the critical angle. The error is ± 0.01 . (d) Refractive index difference ($n_{TM} - n_{TE}$). The estimated error is $\pm 1\%$.

$x \sim 1.5$ as estimated from deposition condition), and this applies to the critical angle in the material. We estimate an experimental error of $\pm 1\%$ for the birefringence. The dispersion of the refractive index in the visible spectral region is one of the factors contributing to this error.

A number of other SiO_x samples on silica substrates were inspected. Two additional examples were found where the TE peaks appear at shorter wavelengths than the TM peaks. One of them is an annealed (1100°C) optical wedge with a lower Si concentration (sample 2) than in sample 1.¹⁵ For sample 2, the birefringence was 1.8% for the highest Si content ($x \sim 1.56$ as estimated from deposition condition) and with an ordinary refractive index $n_o = 1.80$. Another sample is a SiO_x film ($x \sim 1.7$, sample 3) annealed at 1100°C . For this sample, the birefringence was 3.9% ($n_o = 1.85$). Parts of this sample were also annealed at 1150 and 1200°C . Remarkably, the sample annealed at 1150°C shows about twice weaker birefringence than the sample annealed at 1100°C . The sample annealed at 1200°C does

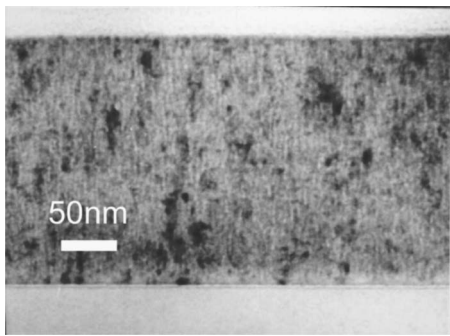


FIG. 4. TEM picture of an annealed SiO_x ($x=1.0\text{--}1.2$) film. The film thickness is 200 nm.

not show any birefringence. The same was observed for several other SiO_x ($x \sim 1.8\text{--}1.85$) samples annealed at 1150°C . From this analysis, we can conclude that the optical birefringence probably occurs in samples with high Si content and annealed at low temperatures.

An annealed 200-nm-thick film with a high Si contents ($x=1.0\text{--}1.2$) was studied using a transmission electron microscope (TEM). The TEM picture clearly shows nonspherical shapes of Si nanostructures (see Fig. 4). The columnlike Si-nc's are mainly oriented perpendicularly to the sample surface. Due to the high residual stress,¹¹ TEM measurements of sample 1 have failed. Based on these experiments, the optical birefringence could be the result of the observed nonspherical shape of the Si-nc. It is possible that birefringent Si-nc's are formed upon annealing at relatively low temperatures (1100°C), and annealing at a high temperature (1200°C) improves the sphericity of Si-nc or/and randomize their orientations, which renders the system optically isotropic.

For the optical wedge with a smaller Si content (sample 2), experiments were also performed in transmission with a He-Ne laser. By using the scheme of crossed polarizers, it is possible to define and analyze the polarization state of the incident and transmitted lights. It was found that this sample turns a linear polarization into an elliptical one so that a transmission can be observed through the crossed polarizers. The transmission increases with the birefringence estimated from the PL measurements. The effect depends on the sample orientation with respect to the polarization of the incident light, and the transmission was maximal when the angle between the Si concentration gradient and the incident polarization is about 45° . This observation supported the concept of optical anisotropy. Sample 3 did not produce any transmission through the crossed polarizers.

B. *m*-line spectra

Figure 5 presents *m*-line curves measured in two different points of sample 1 for each polarization, the Si concentration decreasing from Figs. 5(a) and 5(b). When a good coupling condition is achieved, the two measurements are launched one after the other only by changing the polarization of the light. The signal minima correspond to the values of effective refractive indices. Due to the refractive index of the used prism and also because of the difficulty to couple

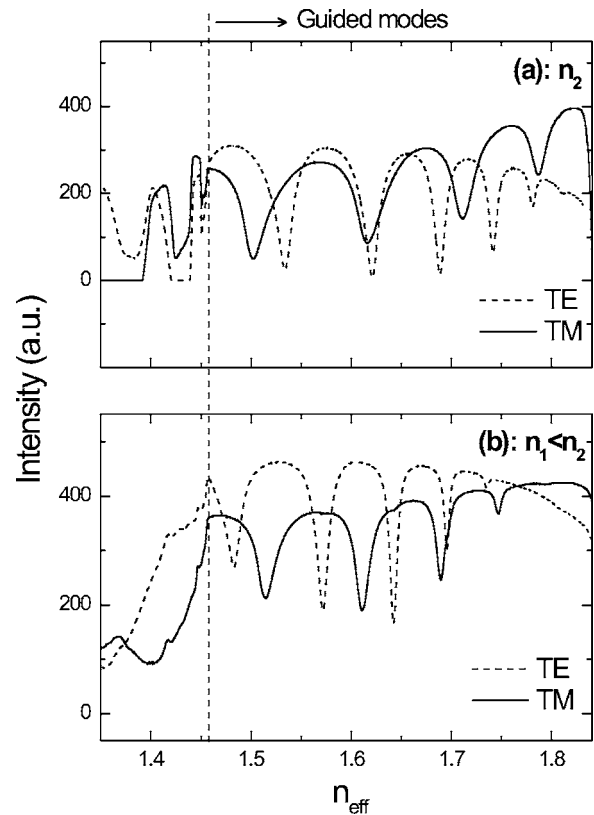


FIG. 5. *m*-line measurements in two points of optical wedge (sample 1). (a) $D=0.5$ cm and (b) $D=2.5$ cm.

the light with low order waveguide modes, not all the waveguide supported modes are observed in our measurements.

In agreement with the PL observations, we found a larger separation of the TM peaks compared to the TE peaks. We focus our efforts on the curves shown in Fig. 5(a), i.e., in the sample zone of a high refractive index. The effective refractive indices for both polarizations can be simulated by using a waveguide simulation code, where the core layer is described by a single and isotropic refractive index. Homogeneous waveguides have the same number of TE and TM modes, the first ones are almost degenerated while the other modes could be separated but always with a larger effective refractive index for the TE modes than for the TM modes. Assuming a step-index profile for the waveguide, we were able to fit the experimental values only for one polarization at once, but never for both together. In these attempts, various refractive index profiles (graded, double wells profile, with barriers, etc.) were tried; however, the situation was qualitatively unchanged.

As a result, it was concluded that it is impossible to reproduce the experimental data using an isotropic refractive index profiles. The only way to simulate the experimental spectra was to assume a rather large positive birefringence and a few missed TM and TE modes in the *m*-line measurements. In order to fit the *m*-line measurements (Fig. 6), the only parameters were the core layer thickness, core layer refractive index, and birefringence. The angle dependence of the propagation index of the extraordinary mode was also taken into account. The best fit shown in Fig. 6 was obtained with 2000 nm thickness, $n_o=1.835$, and 7.5% of positive bi-

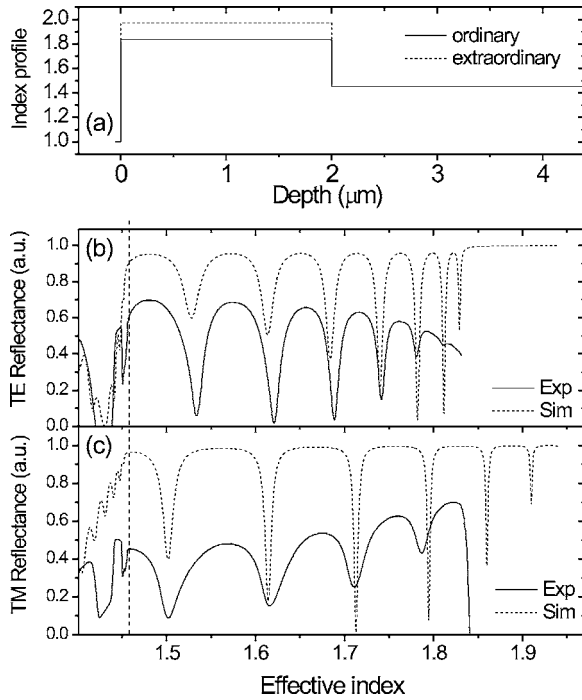


FIG. 6. (a) Refractive index profile extracted from the simulated m -line profiles. [(b) and (c)] Comparison between the measured (line) and simulated (dotted) m -line curves. The measurements were performed at $D = 0.5$ cm. The optical axis of the uniaxial material is assumed to be perpendicular to the layer.

refractive ($n_e = 1.9726$). These parameters agree with the values obtained earlier from PL measurement for this point ($D = 0.5$ cm), where the estimate at the critical angle in the material is achieved. Similar to the PL measurements, the m -line method shows a decrease of birefringence for smaller Si concentrations. It should be mentioned here that the m -line measurements were performed with the 633 nm light, whereas the PL-based measurements are applied to longer wavelengths (~ 800 nm in average). The dependence of the TE refractive index on the orientation of the sample was also studied, showing a maximum variation of $\sim 1\%$ and a higher TE refractive index for light polarization parallel to the direction of the Si concentration gradient. When the TM modes were excited in the m -line measurements, only slight changes were observed as a function of the sample orientation.

In order to obtain the cutoff modes of this structure, the mode spectra for a whole range of wavelengths for $D = 0.5$ cm were calculated (see Fig. 7). These plots show how the modes approach the substrate index (~ 1.455) as a function of the wavelength. The cutoff modes are the ones that reach the left side of the plot. Therefore TE cutoff positions are at 540, 620, 715, 850, and 1040 nm and the TM cutoff positions are at 525, 595, 670, 775, and 910 nm. Cutoff positions for other wavelengths can be also found. These simulations are in agreement with the direct measurements of the cutoff spectrum presented in Fig. 3(a) ($D = 0.5$ cm), which confirms the validity of the models employed here.

A flat SiO_x film (sample 3) was also studied with the m -line method, yielding $n_o = 1.83$ and a birefringence of $\sim 3.5\%$, in agreement with the PL measurements. The main difference with the wedged sample is that the TE refractive

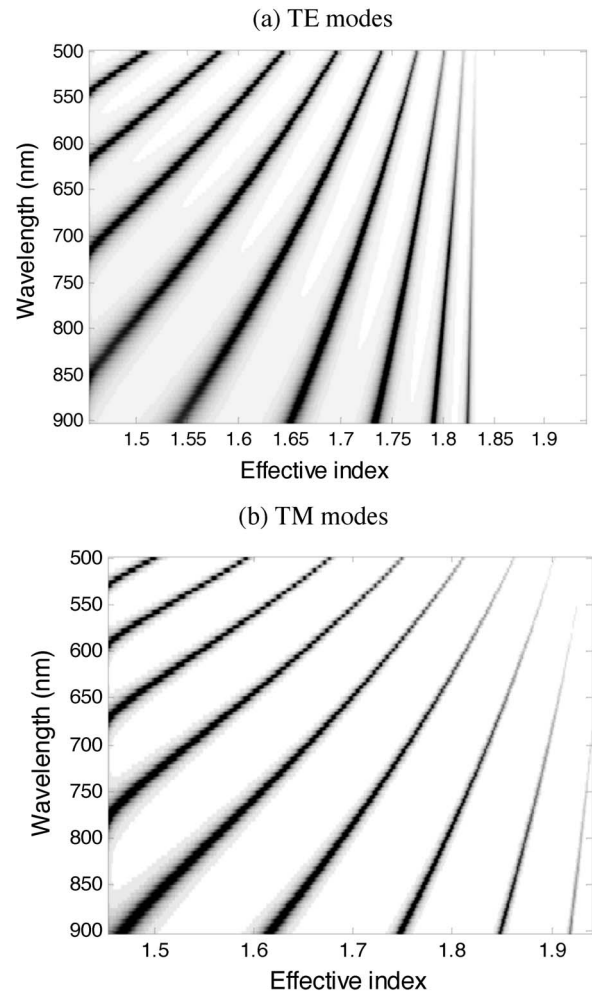


FIG. 7. Mode spectra for a range of wavelengths. It is shown how the modes approach the substrate index (1.455). The cutoff modes are the ones that reach the left side of the plot. The TE cutoff modes are at 540, 620, 715, and 850 nm and the TM cutoff modes are at 525, 595, 670, 775, and 910 nm. The waveguide parameters are those extracted from the fit reported in Fig. 6.

index is independent of the sample orientation with respect to the incident polarization. This result agrees with the measurements with crossed polarizers and it is easily understood in terms of the geometry used to grow this sample. Looking at the index ellipsoids (Fig. 8), we can infer that this homogeneous sample can be represented by an uniaxial material with the optic axis normal to the sample surface, as shown in Fig. 8(a). Birefringence might result from the elongated shape of the single Si-nc.

As what concerns the samples with a refractive index gradient in the plane (samples 1 and 2), there are two possibilities: (i) the material is biaxial with one axis (n_z) oriented perpendicular to the sample surface and the other two directed perpendicular (n_x) and parallel (n_y) to the concentration gradient being $n_z > n_y > n_x$ [see Fig. 8(b)], or (ii) the material is uniaxial with a tilted index ellipsoid, i.e., the optic axis would form an angle with respect to the normal to the sample and, thus, have some projections along the direction of the concentration gradient [see Fig. 8(c)]. The origin of the observed birefringence could be the ellipticity of the Si-nc that in average have similar shapes to the index ellip-

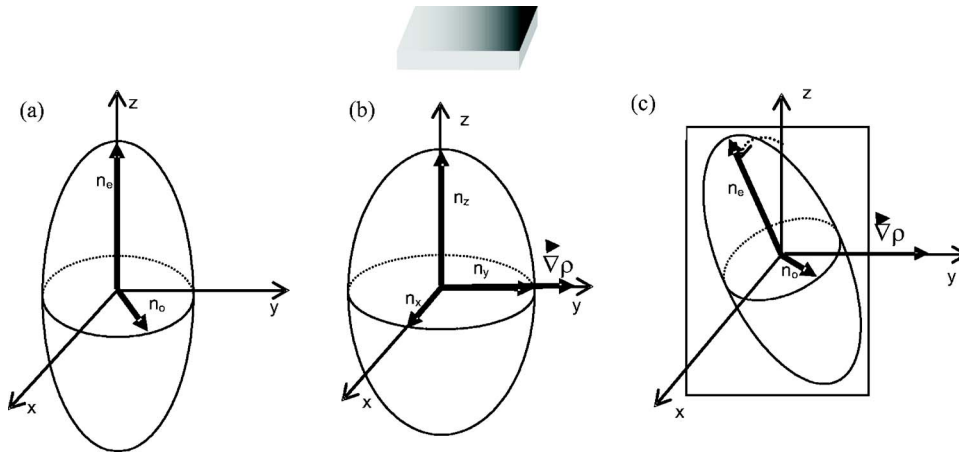


FIG. 8. The index ellipsoid (a) for a homogeneous uniaxial material, (b) for the biaxial inhomogeneous material, and (c) for the tilted uniaxial geometry for inhomogeneous material. $\nabla\rho$ is the concentration gradient in the inhomogeneous material. The sample orientation is shown on the top of the picture. Z direction represents the normal to the sample surface. Case (a) is applicable to sample 3, and samples 1 and 2 are described by either case (b) or case (c).

soid, being a revolution ellipsoid in the case of a uniaxial sample and a squeezed ellipsoid in the case of a biaxial material.

IV. CONCLUSIONS

We have investigated cutoff and *m*-line spectra of several thermally annealed SiO_x films deposited on silica plates. Some of the samples were found to be unusual with respect to the mutual positions of the TE and TM peaks of the guided luminescence. Whereas the theory of asymmetrical waveguides puts the TE cutoff positions at longer wavelengths, the opposite cases were found. Based on the cutoff and *m*-line spectra, this unusual behavior was explained by means of a positive birefringence of the material. For the sample with the highest Si content ($x \sim 1.5$) annealed at 1100 °C, we obtained a maximum birefringence of $\sim 5\%$ from the cutoff spectra and of 7.5% from the *m*-line spectra. The birefringence increases with the Si concentration and decreases at high annealing temperatures (1200 °C). We suggest that nonspherical shapes of Si-nc could be the origin of the observed effect.

The optical parameters (thickness and refractive indices) extracted using the cutoff and *m*-line spectra agree well with each other, which makes the obtained results and the used models confident. The cutoff spectrum simulated based on the parameters extracted from the *m*-line measurements corresponds well to the cutoff spectrum directly measured in the waveguiding detection geometry. In particular, this shows that the filtering effect of the silica layers containing Si-nc can be described within the model of delocalized waveguide modes.

ACKNOWLEDGMENTS

This work was supported by the Academy of Finland (partially by CoE CMS), Gobierno Autónomo de Canarias, Spain (PI042004/018) and by EC through the PHOLOGIC

project (FP6-017158). The authors thank F. Riboli for fruitful discussions and A. Sitnikova for the TEM measurements.

- ¹A. G. Cullis, L. T. Canham, and P. D. J. Calcot, *J. Appl. Phys.* **82**, 909 (1997).
- ²L. Pavesi, *J. Phys.: Condens. Matter* **15**, R1169 (2003).
- ³L. Pavesi, L. Dal Negro, C. Mazzoleni, G. Franzo, and F. Priolo, *Nature (London)* **408**, 440 (2000).
- ⁴L. Khriachtchev, M. Räsänen, S. Novikov, and J. Sinkkonen, *Appl. Phys. Lett.* **79**, 1249 (2001).
- ⁵J. Ruan, P. M. Fauchet, L. Dal Negro, M. Cazzanelli, and L. Pavesi, *Appl. Phys. Lett.* **83**, 5479 (2003).
- ⁶M. Rückschloss, B. Landkammer, and S. Veprek, *Appl. Phys. Lett.* **63**, 1474 (1993).
- ⁷M. V. Wolkov, J. Jorne, P. M. Fauchet, G. Allan, and C. Delerue, *Phys. Rev. Lett.* **82**, 197 (1999).
- ⁸B. T. Sullivan, D. J. Lockwood, H. J. Labbe, and Z.-H. Lu, *Appl. Phys. Lett.* **69**, 3149 (1996).
- ⁹F. Iacona, G. Franzo, and C. Spinella, *J. Appl. Phys.* **87**, 1295 (2000).
- ¹⁰L. Khriachtchev, S. Novikov, and J. Lahtinen, *J. Appl. Phys.* **92**, 5856 (2002).
- ¹¹L. Khriachtchev, M. Räsänen, S. Novikov, and L. Pavesi, *Appl. Phys. Lett.* **85**, 1511 (2004).
- ¹²L. Khriachtchev, M. Räsänen, and S. Novikov, *Appl. Phys. Lett.* **86**, 141911 (2005).
- ¹³L. Khriachtchev, M. Räsänen, and S. Novikov, *Appl. Phys. Lett.* **88**, 013102 (2006).
- ¹⁴L. Khriachtchev, M. Räsänen, and S. Novikov, *Appl. Phys. Lett.* **83**, 3018 (2003).
- ¹⁵L. Khriachtchev, M. Räsänen, S. Novikov, and J. Lahtinen, *J. Appl. Phys.* **95**, 7592 (2004).
- ¹⁶L. Khriachtchev, S. Novikov, J. Lahtinen, and M. Räsänen, *J. Phys.: Condens. Matter* **16**, 3219 (2004).
- ¹⁷J. Valenta, I. Pelant, and J. Linnros, *Appl. Phys. Lett.* **81**, 1396 (2002).
- ¹⁸J. Valenta, I. Pelant, K. Luterova, R. Tomasiunas, S. Cheylan, R. G. Elliman, J. Linnros, and B. Hönerlage, *Appl. Phys. Lett.* **82**, 955 (2003).
- ¹⁹J. Valenta, T. Ostatnický, I. Pelant, R. G. Elliman, J. Linnros, and B. Hönerlage, *J. Appl. Phys.* **96**, 5222 (2004).
- ²⁰I. Pelant, T. Ostatnický, J. Valenta, K. Luterova, E. Skopalova, T. Mates, and R. G. Elliman, *Appl. Phys. B: Lasers Opt.* **83**, 87 (2006).
- ²¹P. K. Tien, *Appl. Opt.* **10**, 2395 (1971).
- ²²H. G. Unger, *Planar Optical Waveguides and Fibers* (Clarendon, Oxford, 1977).
- ²³H. Kogelnik and V. Ramaswamy, *Appl. Opt.* **13**, 1857 (1974).
- ²⁴A. V. Subashiev and S. Luryi, *J. Lightwave Technol.* **24**, 1513 (2006).